Frontiers of Physics
https://doi.org/10.1007/s11467-018-0858-z
Front. Phys.
14(1), 13602 (2019)

RESEARCH ARTICLE

Tuning up-conversion luminescence in Er^{3+}-doped glass ceramic by phase-shaped femtosecond laser field with optimal feedback control

Lian-Zhong Deng[1,*], Yun-Hua Yao[1,*], Li Deng[1,*], Huai-Yuan Jia[4], Ye Zheng[1], Cheng Xu[2], Jian-Ping Li[1], Tian-Qing Jia[1], Jian-Rong Qiu[2], Zhen-Rong Sun[1], Shi-An Zhang[1,3,†]

[1] *State Key Laboratory of Precision Spectroscopy, East China Normal University, Shanghai 200062, China*
[2] *State Key Laboratory of Silicon Materials, Zhejiang University, Hangzhou 310027, China*
[3] *Collaborative Innovation Center of Extreme Optics, Shanxi University, Taiyuan 030006, China*
[4] *State Key Laboratory of Robatics, Shenyang Institute of Automation, Chinese Academy of Sciences, Shenyang 110016, China*
Corresponding author. Email: [†] *sazhang@phy.ecnu.edu.cn*
Received June 5, 2018; accepted August 22, 2018

Tuning the color output of rare-earth ion doped luminescent nanomaterials has important scientific significance for further extending applications in color displays, laser sources, optoelectronic devices, and biolabeling. In previous studies, pre-designed phase modulation of the femtosecond laser field has been proven to be effective in tuning the luminescence of doped rare-earth ions. Owing to the complex light–matter interaction in the actual experiment, the dynamic range and optimal efficiency for color tuning cannot be determined with the pre-designed phase modulation. This article shares the development of an adaptive femtosecond pulse shaping method based on a genetic algorithm, and its use to manipulate the green and red luminescence tuning in an Er^{3+}-doped glass ceramic under 800-nm femtosecond laser field excitation for the first time. Experimental results show that the intensity ratio of the green and red UC luminescence of the doped Er^{3+} ions can be either increased or decreased conveniently by the phase-shaped femtosecond laser field with an optimal feedback control. The physical control mechanisms for the color tuning are also explained in detail. This article demonstrates the potential applications of the adaptive femtosecond pulse shaping technique in controlling the color output of doped rare-earth ions.

Keywords nonlinear optics, upconversion luminescence, rare earth ions, luminescent nanomaterials

1 Introduction

Tuning the color output of the rare-earth ion doped luminescent nanomaterials has attracted considerable attention of researchers due to its important applications in many related areas, such as color display [1, 2], laser source [3, 4], optoelectronic devices [5, 6], and biolabeling [7, 8]. Up to now, various schemes have been proposed to realize color output tuning in rare-earth ion doped luminescent nanomaterials. Changing the material property is a common method, such as varying the lanthanide dopant [9, 10], dopant concentration [11, 12], particle size [13, 14], morphology [15–17], core-shell structure [18–20], and surface-plasmon coupling [21–23]. Modulating the surrounding environment is another strategy, such as applying an electric [24] and magnetic field [25, 26], or adjusting the sample temperature [27, 28]. Varying the excitation source is considered as the other common method, such as controlling the excitation wavelength [29], power density [30, 31], repetition rate [32], pulse duration [33] and spectral phase [34–36], or employing a two-color laser field [37, 38]. Compared to changing the material property or modulating the surrounding environment, varying the excitation source has a major advantage in that the color output tuning can be controlled in a real-time and reversible manner.

In our previous studies, the green and red up-conversion (UC) luminescence in Er^{3+}-doped glass ceramic were both suppressed by shaping the femtosecond laser field with a pre-designed square phase modulation [36]. However, the dynamic range and optimal efficiency for the color tuning could not be fully explored with the pre-designed phase modulation. Therefore, we developed an adaptive femtosecond pulse shaping system based on a genetic algorithm (GA) with a feedback control strategy, and used it to control the UC luminescence of the rare-earth ion doped luminescent nanomaterials for the first time. The GA based optimal control method can automatically look for the direction in the searching space and obtain the global solution. The method has been actively used in manipulating both physical and chemical processes, and

*These authors contributed equally to this work.

© Higher Education Press and Springer-Verlag GmbH Germany, part of Springer Nature 2019

serves as an unprecedented means to explore the quantum dynamics of such processes [39–45].

By using the femtosecond pulse shaping system with the optimal feedback control based on GA, the experimental investigation of green and red UC luminescence tuning in Er^{3+}-doped glass ceramic was conducted. The experimental study indicates that the intensities of green and red UC luminescence can be either increased or decreased effectively and their ratio can be tuned by shaping the femtosecond laser field with the phase modulation. The tentative physical control mechanisms for the green and red UC luminescence tuning are also explained based on the current observations and previous works.

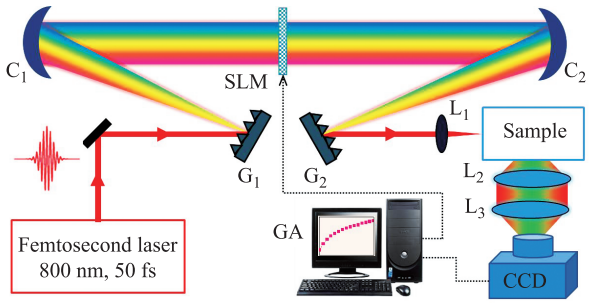


Fig. 1 The experimental arrangement of the adaptive femtosecond laser pulse shaping system based on genetic algorithm. Here, SLM is spatial light modulator, G_1 and G_2 are diffraction gratings, C_1 and C_2 are cylindrical concave mirrors, L_1, L_2, and L_3 are focusing lenses, and CCD is spectrometer with charged-coupled device.

2 Experimental setup

The experimental arrangement of the adaptive femtosecond pulse shaping system is schematically shown in Fig. 1. A Ti-sapphire mode-locked regenerative amplifier (Spitfire, Spectra Physics) is used as the excitation source with the central wavelength of 800 nm, pulse width of about 35 fs and repetition rate of 1 kHz. The femtosecond laser pulse is sent into a programmable 4f configuration zero-dispersion pulse shaper, which consists of a pair of diffraction gratings of 1200 lines/mm (G_1 and G_2), a pair of cylinder concave mirrors of 200 mm focal length (C_1 and C_2) and a one-dimension liquid-crystal spatial light modulator (SLM-S320d, JENOPTIK). The SLM is located at the Fourier plane of the pulse shaping system and used to vary the spectral phase in the frequency domain. The output femtosecond laser pulse is then focused into the sample via a lens of 50 mm focus length (L1). The peak intensity of the transform-limited (TL) (unmodulated) femtosecond laser pulse in the sample is estimated to be about 8.3×10^{12} W/cm^2. The phase modulation doesn't affect the total energy of the laser pulse, but might greatly change the peak laser intensity. All luminescence signals radiating from the sample are collected by a telescope system consisting of a pair of lenses (L_2 and L_3), and measured by a spectrometer with charged-coupled device (CCD). Both the SLM and spectrometer are connected to a personal computer (PC) for control. A GA based feedback control program is utilized to optimize the luminescence intensity by controlling the spectral phase of the femtosecond laser field.

The adaptive feedback control program based on GA is shown in Fig. 2. The GA is a conventional optimization algorithm, which is inspired by the process of natural selection and genetics. In the GA-based optimization process, the candidate population is evolved toward better solutions. Typically, the GA requires a genetic representation of the solution domain, and utilizes a fitness function to evaluate it. Normally, the binary arrays are used to represent the solution domain for easier operation. Figure 2(a) shows the flow chart of the GA-based program in our experiment. Here, five procedures are included in the program, which are initialization, evaluation, selection, genetic operation and termination. In the initialization, a group of individuals are randomly generated, i.e. the first

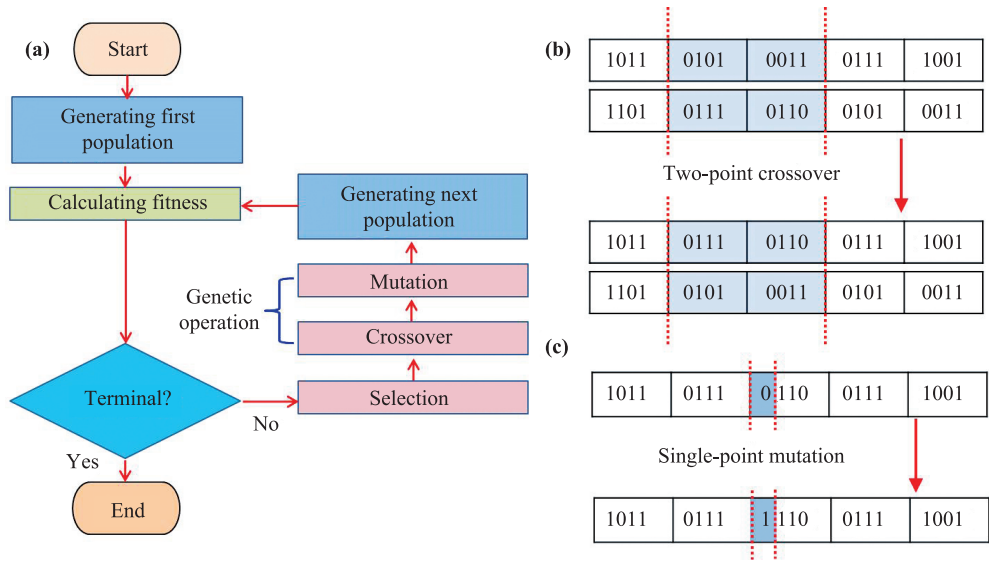


Fig. 2 **(a)** The flow chart of the GA-based program for feedback control in our experiment. The operation methods of the two-point crossover **(b)** and single-point mutation **(c)**.

generation. Then, each individual is evaluated according to its fitness. Here, the intensity ratio of the green and red UC luminescence is used as the fitness function. A number of good individuals are selected and used as parents for the next generation. In the genetic operation, a new generation is formed from these parents via crossover and mutation. In our experiment, the two-point crossover mode and single-point mutation mode are found to work well, as shown in Figs. 2(b) and (c), respectively. Similarly, the new generation is also individually evaluated according to its fitness. The above process is repeatedly performed until the fitness function approaches convergence.

The experiment is performed in 5%Er^{3+}-doped NaYF4 nanocrystals dispersed in silicate glass with the composition of 40SiO_2-25Al_2O_3-18Na_2CO_3-10YF_3-7NaF-5ErF_3 (mol.%). The original materials are mixed and melted in a covered platinum crucible at the temperature of 1450° for 45 min in the ambient atmosphere, and then are cast into a brass mold followed by annealing at the temperature of 450° for 10 h. The synthesized glass is heated to the temperature of 600° with an increase rate of 10 K/min, kept at this temperature for 2 h, and then cooled down to room temperature to form the glass ceramic through crystallization. Finally, the sample is cut and polished for optical measurement in our experiment.

3 Results and discussion

The UV-VIS-NIR absorption spectrum of Er^{3+}-doped glass ceramic is shown in Fig. 3(a), which is measured by a spectrophotometer (TU-1901, Purkinje). There are seven main absorption bands with the central wavelengths around 377, 407, 487, 518, 542, 651 and 799 nm, which can be attributed to the state transitions from the ground state $^4I_{15/2}$ to these excited states $^4G_{11/2}$, $^2H_{9/2}$, $^4F_{7/2}$, $^2H_{11/2}$, $^4S_{3/2}$, $^4F_{9/2}$ and $^4I_{9/2}$, respectively. The UC luminescence spectrum in the visible light region under the excitation of 800 nm femtosecond laser field is shown in Fig. 3(b). One can see that five luminescence peaks can be observed around the wavelengths of 408, 475, 527, 546 and 656 nm, which can be assigned to the state transitions from these excited states $^2H_{9/2}$, $^4F_{7/2}$, $^2H_{11/2}$, $^4S_{3/2}$, $^4F_{9/2}$ to the ground state $^4I_{15/2}$, respectively. It is noted that the green (around 546 nm) and red (around 656 nm) UC luminescence dominate the visible light spectrum.

Firstly, we analyze the UC excitation process for the green and red UC luminescence. Figure 4(a) shows the energy level diagram of Er^{3+} ions and the possible UC excitation processes for the green and red luminescence generation under the TL femtosecond laser field. When the glass ceramic sample is irradiated by the unshaped femtosecond laser pulse, the population in the ground state $^4I_{15/2}$ is excited into the excited state $^4H_{9/2}$ by resonance-mediated two-photon absorption (TPA). This TPA process can be decomposed into two parts: on-resonant part and near-resonant part [34]. The on-resonant part represents the TPA process via the intermediate state $^4I_{9/2}$. That is, the population in the ground state $^4I_{15/2}$ is first excited to the intermediate state $^4I_{9/2}$ by absorbing a photon, and is then further excited to the higher state $^4H_{9/2}$ by absorbing another photon from the same laser pulse. The near-resonant part corresponds to all other absorption processes not via the intermediate state $^4I_{9/2}$. That is, the population in the ground state $^4I_{15/2}$ is directly excited to the excited state $^4H_{9/2}$ by simultaneously absorbing two photons from the same laser pulse. Here, the sum of the two photon energies is equal to the energy gap of the two states of $^4H_{9/2}$ and $^4I_{15/2}$. The population in the excited state $^4H_{9/2}$ can nonradiatively relax to the three lower excited states of $^2H_{11/2}$, $^4S_{3/2}$ and $^4F_{9/2}$, then further decays back to the ground state $^4I_{15/2}$, and finally emits the green and red fluorescence. Another UC excitation process for the green and red luminescence generation involves the single-photon absorption (SPA) followed by an energy transfer up-conversion (ETU) process. The population in the ground state $^4I_{15/2}$ is first pumped to the

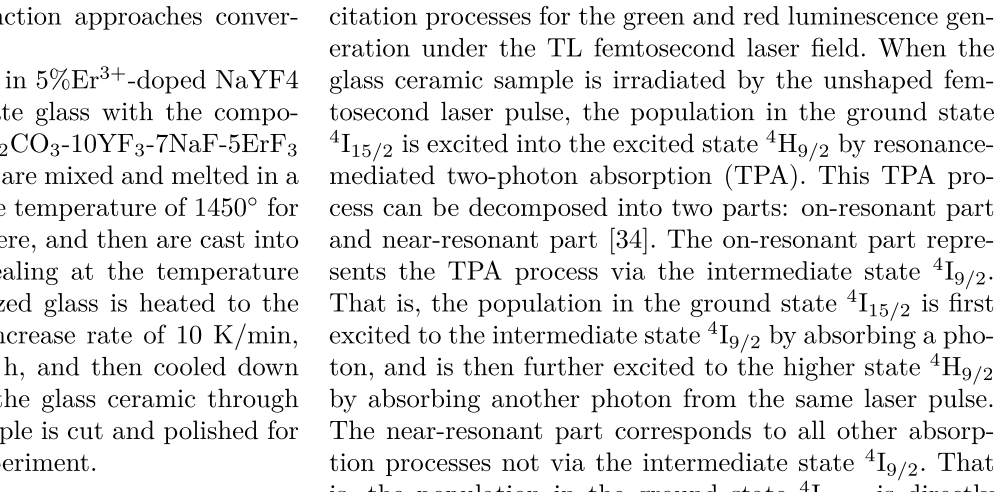


Fig. 3 **(a)** The UV-VIS-NIR absorption spectrum of Er^{3+}-doped glass ceramic. **(b)** The up-conversion luminescence spectrum in the visible light region under the excitation of 800 nm femtosecond laser.

excited state $^4I_{9/2}$ by the SPA process, and then the population in the excited state $^4I_{9/2}$ spontaneously relaxes to the two lower excited states of $^4I_{11/2}$ and $^4I_{13/2}$. Since the dopant concentration of Er^{3+} ions is as high as 5%, the ETU process between neighboring Er^{3+} ions can occur via the two state transitions of $^4I_{11/2}+{}^4I_{11/2} \rightarrow {}^4I_{15/2}+{}^4F_{7/2}$ (ETU1) and $^4I_{11/2} + {}^4I_{13/2} \rightarrow {}^4I_{15/2}+{}^4F_{9/2}$ (ETU2). The population in the excited state $^4F_{7/2}$ can nonradiatively relax to the lower states of $^2H_{11/2}$, $^4S_{3/2}$ and $^4F_{9/2}$ and also emit the green and red fluorescence by further decaying back to the ground state $^4I_{15/2}$. However, the population in the excited state $^4F_{9/2}$ can only emit the red fluorescence when it decays back to the ground state $^4I_{15/2}$. It can be concluded that the green UC luminescence mainly comes from the excitation processes of TPA and ETU1 while the red UC luminescence mainly results from the contributions of the TPA, ETU1 and ETU2 processes. As shown in Fig. 4(a), since the green and red UC luminescence come from the different UC excitation pathways, their intensities can be tuned if these excitation processes are appropriately controlled. Here, we try to accomplish this purpose by adaptively shaping the spectral phase of the femtosecond laser field.

In the first experiment, we set the intensity ratio of the green (546 nm) and red (656 nm) UC luminescence, denoted as I_{546}/I_{656}, as the fitness function, and optimize the spectral phase distribution to increase the ratio. For better search of the global solution, the crossover and mutation rates are adaptively varied. The total population number for each generation is 200 with 5 of the most optimal selected out as parents of the next generation. A large number of test trails with various initial phases are performed, and majority of them succeed in producing similar results as those presented in Fig. 5. The intensity ratio I_{546}/I_{656} in the optimization process first increases rapidly and then approaches a stable value, as shown in Fig. 5(a). After optimization, the intensity ratio is increased from 2.23 to 2.89. For direct comparison, the green and red UC luminescence spectra with and without phase optimization are plotted in Fig. 5(b). As can be seen, both

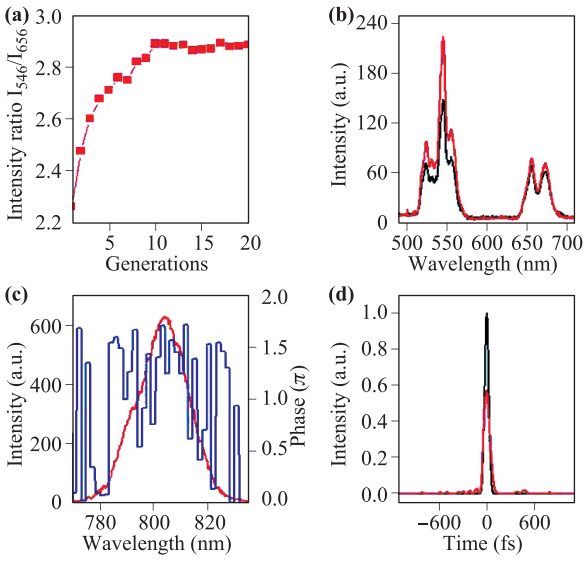


Fig. 5 **(a)** The intensity ratio (I_{546}/I_{656}) maximization process. **(b)** The enhanced (red line) and unmodulated (black line) up-conversion luminescence spectra. **(c)** The optimal phase distribution, together with the laser spectrum. **(d)** The temporal intensity distribution of the shaped (red line) and unshaped (black line) femtosecond laser fields.

the green and red UC luminescence are enhanced with the optimal control. But the green UC luminescence obtains a larger enhancement efficiency than the red one. The finally optimized phase distributions for the successful test trials are also checked to be nearly the same, as shown in Fig. 5(c). Based on the results of Fig. 5(c) the temporal intensity distribution of the shaped femtosecond laser field is calculated and shown in Fig. 5(d) (red line). The time profile of the unshaped (i.e., TL) laser pulse is also plotted for comparison (black line). As one can see, the femtosecond laser pulse with the optimal phase modulation is slightly broadened and a series of rather weak subpulses are around the main peak.

Early in 2000, Dudovich *et al.* have proposed and demonstrated that the TL femtosecond laser pulse is not optimal for the resonant multi-photon transitions, which can be enhanced significantly by properly controlling the spectral phase distribution [46]. Recently, our theoretical study has shown that an appropriate rectangle phase modulation can enhance the resonance-mediated TPA in Er^{3+} ions [47]. Therefore, we dare to explain the physical control mechanisms for the observed luminescence enhancement. In the resonance-mediated TPA process, the on-resonant part mainly comes from the contribution of the central frequency components, while the near-resonant part mainly results from the excitation of low and high laser frequency components. The phase modulation in Fig. 5(c) can induce a constructive interference between the excitation pathways of the on-resonant and near-resonant TPA processes, and finally increases the TPA probability. The ETU process is, however, related

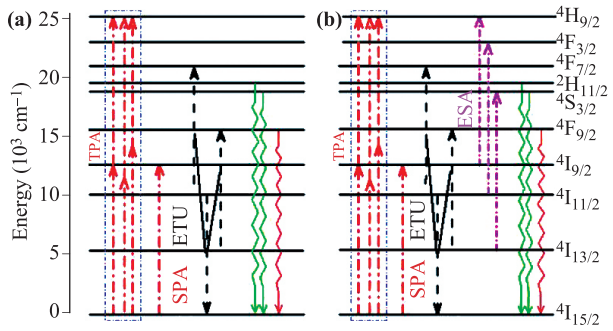


Fig. 4 The energy level diagram of Er^{3+} ions and the possible up-conversion processes for **(a)** unshaped femtosecond laser field and **(b)** the shaped femtosecond laser field with a sequence of subpulses.

to the SPA process. Since the phase modulation does not affect the total energy of the laser pulse, the total probability of the SPA process is assumed to remain unchanged and so is the total probability of the ETU process. As a result, both the green and red UC luminescence are enhanced. The weight of TPA in the whole excitation process determines the enhancement efficiency of the UC luminescence. The higher the weight, the larger the enhancement efficiency. Compared with the green UC luminescence, the red UC luminescence additionally contains the ETU2 process. Thus, the TPA contribution in the red UC excitation process is relatively low. Correspondingly, the enhancement efficiency of the red UC luminescence is also relatively small.

In the second experiment, we optimize the spectral phase distribution to decrease the intensity ratio I_{546}/I_{656}, and the experimental results are shown in Fig. 6. After optimizing the spectral phase, the intensity ratio I_{546}/I_{656} is reduced from 2.23 to 1.51, as shown in Fig. 6(a). The green and red UC luminescence spectra before and after the phase optimization are shown in Fig. 6(b). It can be seen that the green UC luminescence intensity decreases while the red UC luminescence intensity increases. Similarly, the optimal phase distribution in the frequency domain is checked and given in Fig. 6(c). The temporal intensity distribution of the shaped femtosecond laser field is correspondingly calculated and shown in Fig. 6(d) (red line). As one can see, with the optimal phase modulation, the femtosecond laser pulse is now tailored into a sequence of subpulses. These subpulses are separated in a time range of picoseconds and have comparable peak intensities.

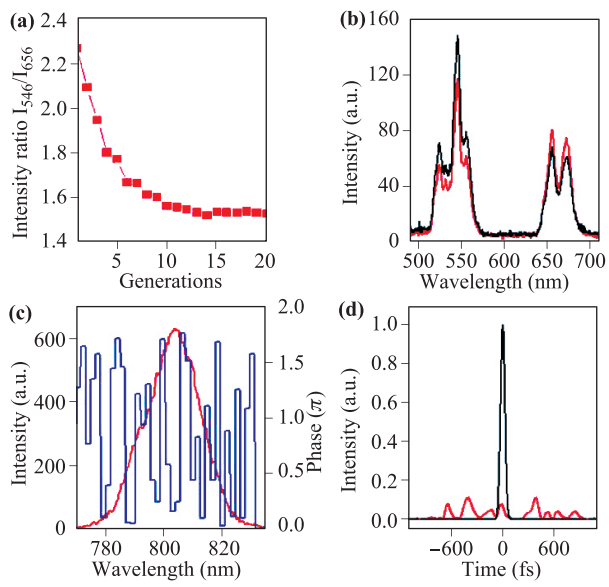


Fig. 6 **(a)** The intensity ratio (I_{546}/I_{656}) minimization process. **(b)** The suppressed (red line) and unmodulated (black line) up-conversion luminescence spectra. **(c)** The optimal phase distribution, together with the laser spectrum. **(d)** The temporal intensity distribution of the shaped (red line) and unshaped (black line) femtosecond laser fields.

With the time extension of the shaped femtosecond laser pulse, the TPA process will be greatly suppressed and an excited state absorption (ESA) process can occur. These ESA processes were first experimentally studied in our previous work, which reported on the suppression of UC luminescence in Er^{3+}-doped glass ceramic by shaping the laser pulse with a pre-designed square phase modulation [36]. The UC excitation processes are now as shown in Fig. 4(b). In the ESA processes, the populations in the three excited states $^4I_{9/2}$, $^4I_{11/2}$ and $^4I_{13/2}$ can be further pumped to the higher three excited states $^4H_{9/2}$, $^4F_{3/2}$ and $^4S_{3/2}$ by absorbing another photon from subsequent subpulses, respectively. The populations in the three excited states $^4H_{9/2}$, $^4F_{3/2}$, and $^4S_{3/2}$ will relax and finally decay to the ground state $^4I_{15/2}$, emitting the green and red UC luminescence. Since the impact of the phase modulation on the ETU process is ignorable, as discussed above, the change of the UC luminescence intensity now depends on the combined contributions of TPA and ESA processes. For the green UC luminescence, the new contribution of ESA is less than the decrement of the suppressed TPA, and therefore its intensity is decreased. However, the new contribution of ESA is larger than the decrement of the suppressed TPA for the red UC luminescence, and thus its intensity is increased.

In the actual experiment, the physical control processes may be more complex. The adaptive femtosecond pulse shaping method has the advantage that it can automatically search for the optimal spectral phase distribution without the related information about the control system. Based on the optimal phase distribution, one can develop or explore some new physical control processes for the UC luminescence of rare-earth ions in the future study.

4 Conclusions

In conclusions, we have reported an adaptive femtosecond pulse shaping method based on GA to control the green and red UC luminescence tuning in the Er^{3+} doped glass ceramic within a wide dynamic range. Our results have shown that the intensity ratio of the green and red UC luminescence can be either increased or decreased conveniently by using the optimal feedback control strategy. The physical control mechanisms for the observed green and red luminescence tuning have also been properly explained. The femtosecond pulse shaping method with the optimal feedback control has been shown to be a powerful studying tool in many research areas involving laser-matter interactions [45]. To our knowledge, it has never been applied to control the UC luminescence of the rare-earth ion doped solid materials before. This work has demonstrated for the first time that the adaptive femtosecond pulse shaping method is a useful tool to auto-

matically optimize the UC luminescence control in rare-earth ion doped luminescent nanomaterials and is quite meaningful for future studies in many related application areas, such as color tuning, fluorescence imaging and photoelectric conversion.

Acknowledgements Financial supports from the National Natural Science Foundation of China (Grant Nos. 11727810, 61720106009, and 11774094) and Science and Technology Commission of Shanghai Municipality (Grant Nos. 17ZR146900 and 16520721200) are gratefully acknowledged

References

1. E. Downing, L. Hesselink, J. Ralston, and R. Macfarlane, A three-color, solid-state, three-dimensional display, *Science* 273(5279), 1185 (1996)
2. R. Deng, F. Qin, R. Chen, W. Huang, M. Hong, and X. Liu, Temporal full-colour tuning through non-steady-state upconversion, *Nat. Nanotechnol.* 10(3), 237 (2015)
3. J. Nilsson, W. A. Clarkson, R. Selvas, J. K. Sahu, P. W. Turner, S. Alam, and A. B. Grudinin, High-power wavelength-tunable cladding-pumped rare-earth-doped silica fiber lasers, *Opt. Fiber Technol.* 10(1), 5 (2004)
4. E. Wintner, E. Sorokin, and I. T. Sorokina, Recent developments in diode-pumped ultrashort pulse solid-state Lasers, *Laser Phys.* 11(11), 1193 (2001)
5. L. Wang, Y. Li, Y. Zhang, H. Gu, and W. Chen, Rare earth compound nanowires: Synthesis, properties and applications, *Rev. Nanosci. Nanotechnol.* 3(1), 1 (2014)
6. T. Zhong, J. M. Kindem, E. Miyazono, and A. Faraon, Nanophotonic coherent light-matter interfaces based on rare-earth-doped crystals, *Nat. Commun.* 6(1), 8206 (2015)
7. F. Wang, W. B. Tan, Y. Zhang, X. Fan, and M. Wang, Luminescent nanomaterials for biological labeling, *Nanotechnology* 17(1), R1 (2006)
8. E. Wolska, J. Kaszewski, P. Kiełbik, J. Grzyb, M. M. Godlewski, and M. Godlewski, Rare earth activated ZnO nanoparticles as biomarkers, *Opt. Mater.* 36(10), 1655 (2014)
9. S. Han, R. Deng, X. Xie, and X. Liu, Enhancing luminescence in lanthanide-doped upconversion nanoparticles, *Angew. Chem. Int. Ed.* 53(44), 11702 (2014)
10. S. Heer, K. Kömpe, H. U. Güdel, and M. Haase, Highly efficient multicolour upconversion emission in transparent colloids of lanthanide-doped $NaYF_4$ nanocrystals, *Adv. Mater.* 16(23–24), 2102 (2004)
11. F. Wang and X. Liu, Upconversion multicolor fine-tuning: visible to near-infrared emission from lanthanide-doped $NaYF_4$ nanoparticles, *J. Am. Chem. Soc.* 130(17), 5642 (2008)
12. F. Wang, X. Xue, and X. Liu, Multicolor Tuning of (Ln, P)-Doped YVO_4 nanoparticles by single-wavelength excitation, *Angew. Chem. Int. Ed.* 47(5), 906 (2008)
13. X. Bai, H. Song, G. Pan, Y. Lei, T. Wang, X. Ren, S. Lu, B. Dong, Q. Dai, and L. Fan, Size-dependent upconversion luminescence in Er^{3+}/Yb^{3+}-codoped nanocrystalline yttria: Saturation and thermal effects, *J. Phys. Chem. C* 111(36), 13611 (2007)
14. Y. Sheng, L. Liao, A. Bandla, Y. Liu, N. Thakor, and M. C. Tan, Size and shell effects on the photoacoustic and luminescence properties of dual modal rare-earth-doped nanoparticles for infrared photoacoustic imaging, *ACS Biomater Sci. & Eng.* 2(5), 809 (2016)
15. Y. Sun, Y. Chen, L. Tian, Y. Yu, X. Kong, J. Zhao, and H. Zhang, Controlled synthesis and morphology dependent upconversion luminescence of $NaYF_4$:Yb, Er nanocrystals, *Nanotechnology* 18(27), 275609 (2007)
16. J. Silver, M. I. Martinez-Rubio, T. G. Ireland, G. R. Fern, and R. Withnall, The effect of particle morphology and crystallite size on the upconversion luminescence properties of erbium and ytterbium co-doped yttrium oxide phosphors, *J. Phys. Chem. B* 105(5), 948 (2001)
17. Z. Bai, H. Lin, J. Johnson, S. C. R. Gui, K. Imakita, R. Montazami, M. Fujii, and N. Hashemi, The single-band red upconversion luminescence from morphology and size controllable Er^{3+}/Yb^{3+} doped MnF_2 nanostructures, *J. Mater. Chem. C* 2(9), 1736 (2014)
18. G. Yi and G. Chow, Water-soluble $NaYF_4$:Yb, Er (Tm)/$NaYF_4$/polymer core/shell/shell nanoparticles with significant enhancement of upconversion fluorescence, *Chem. Mater.* 19(3), 341 (2007)
19. F. Wang, R. Deng, J. Wang, Q. Wang, Y. Han, H. Zhu, X. Chen, and X. Liu, Tuning upconversion through energy migration in core-shell nanoparticles, *Nat. Mater.* 10(12), 968 (2011)
20. X. Chen, D. Peng, Q. Ju, and F. Wang, Photon upconversion in core-shell nanoparticles, *Chem. Soc. Rev.* 44(6), 1318 (2015)
21. W. Feng, L. Sun, and C. Yan, Ag nanowires enhanced upconversion emission of $NaYF_4$: Yb, Er nanocrystals via a direct assembly method, *Chem. Commun.* 0(29), 4393 (2009)
22. S. Schietinger, T. Aichele, H. Wang, T. Nann, and O. Benson, Plasmon-enhanced upconversion in single $NaYF_4$: Yb^{3+}/Er^{3+} codoped nanocrystals, *Nano Lett.* 10(1), 134 (2010)
23. H. Zhang, D. Xu, Y. Huang, and X. Duan, Highly spectral dependent enhancement of upconversion emission with sputtered gold island films, *Chem. Commun.* 47(3), 979 (2011)
24. J. Hao, Y. Zhang, and X. Wei, Electric-induced enhancement and modulation of upconversion photoluminescence in epitaxial $BaTiO_3$:Yb/Er thin films, *Angew. Chem.* 123(30), 7008 (2011)
25. Y. Liu, D. Wang, J. Shi, Q. Peng, and Y. Li, Magnetic tuning of upconversion luminescence in lanthanide-doped bifunctional nanocrystals, *Angew. Chem. Int. Ed.* 52(16), 4366 (2013)

26. P. Chen, Z. Zhong, H. Jia, J. Zhou, J. Han, X. Liu, and J. Qiu, Magnetic field enhanced upconversion luminescence and magnetic-optical hysteresis behaviors in $NaYF_4$: Yb, Ho nanoparticles, *RSC Advances* 6(9), 7391 (2016)
27. B. Dong, B. Cao, Y. He, Z. Liu, Z. Li, and Z. Feng, Temperature sensing and in vivo imaging by molybdenum sensitized visible upconversion luminescence of rare-earth oxides, *Adv. Mater.* 24(15), 1987 (2012)
28. F. Vetrone, R. Naccache, A. Zamarrón, A. Juarranz De La Fuente, F. Sanz-Rodríguez, L. Martinez Maestro, E. Martín Rodriguez, D. Jaque, J. García Solé, and J. A. Capobianco, Temperature sensing using fluorescent nanothermometers, *ACS Nano* 4(6), 3254 (2010)
29. G. Franzò, F. Iacona, V. Vinciguerra, and F. Priolo, Enhanced rare earth luminescence in silicon nanocrystals, *Mater. Sci. Eng. B* 69–70, 335 (2000)
30. X. Xue, M. Thitsa, T. Cheng, W. Gao, D. Deng, T. Suzuki, and Y. Ohishi, Laser power density dependent energy transfer between Tm^{3+} and Tb^{3+}: tunable upconversion emissions in $NaYF_4$: Tm^{3+}, Tb^{3+}, Yb^{3+} microcrystals, *Opt. Express* 24(23), 26307 (2016)
31. C. Zhang, L. Yang, J. Zhao, B. Liu, M. Y. Han, and Z. Zhang, White-light emission from an integrated upconversion nanostructure: Toward multicolor displays modulated by laser power, *Angew. Chem. Int. Ed.* 54(39), 11531 (2015)
32. C. F. Gainer, G. S. Joshua, and M. Romanowski, Toward the use of two-color emission control in upconverting $NaYF_4$:Er^{3+},Yb^{3+} nanoparticles for biomedical imaging, *Proc. SPIE* 8231, 82310I, 82310I-8 (2012)
33. C. F. Gainer, G. S. Joshua, C. R. De Silva, and M. Romanowski, Control of green and red upconversion in $NaYF_4$: Yb^{3+}, Er^{3+} nanoparticles by excitation modulation, *J. Mater. Chem.* 21(46), 18530 (2011)
34. S. Zhang, C. Lu, T. Jia, J. Qiu, and Z. Sun, Coherent phase control of resonance-mediated two-photon absorption in rare-earth ions, *Appl. Phys. Lett.* 103(19), 194104 (2013)
35. Y. Yao, S. Zhang, H. Zhang, J. Ding, T. Jia, J. Qiu, and Z. Sun, Laser polarization and phase control of upconversion fluorescence in rare-earth ions, *Sci. Rep.* 4(1), 7295 (2015)
36. S. Zhang, Y. Yao, X. S. Wu, P. Liu, J. Ding, T. Jia, J. Qiu, and Z. Sun, Realizing up-conversion fluorescence tuning in lanthanide-doped nanocrystals by femtosecond pulse shaping method, *Sci. Rep.* 5(1), 13337 (2015)
37. P. Chen, S. Yu, B. Xu, J. Wang, X. Sang, X. Liu, and J. Qiu, Enhanced upconversion luminescence in $NaYF_4$: Er nanoparticles with multi-wavelength excitation, *Mater. Lett.* 128, 299 (2014)
38. Y. Yao, C. Xu, Y. Zheng, C. Yang, P. Liu, J. Ding, T. Jia, J. Qiu, S. Zhang, and Z. Sun, Enhancing up-conversion luminescence of Er^{3+}/Yb^{3+}-codoped glass by two-color laser field excitation, *RSC Advances* 6(5), 3440 (2016)
39. S. Lee, K. Jung, J. H. Sung, K. Hong, and C. H. Nam, Adaptive quantum control of DCM fluorescence in the liquid phase, *J. Chem. Phys.* 117(21), 9858 (2002)
40. A. Assion, T. Baumert, M. Bergt, T. Brixner, B. Kiefer, V. Seyfried, M. Strehle, and G. Gerber, Control of chemical reactions by feedback-optimized phase-shaped femtosecond laser pulses, *Science* 282(5390), 919 (1998)
41. R. J. Levis, G. M. Menkir, and H. Rabitz, Selective bond dissociation and rearrangement with optimally tailored, strong-field laser pulses, *Science* 292(5517), 709 (2001)
42. R. Bartels, S. Backus, E. Zeek, L. Misoguti, G. Vdovin, I. P. Christov, M. M. Murnane, and H. C. Kapteyn, Shaped-pulse optimization of coherent emission of high-harmonic soft X-rays, *Nature* 406(6792), 164 (2000)
43. M. Aeschlimann, M. Bauer, D. Bayer, T. Brixner, F. J. G. De Abajo, W. Pfeiffer, M. Rohmer, C. Spindler, and F. Steeb, Adaptive subwavelength control of nano-optical fields, *Nature* 446(7133), 301 (2007)
44. J. L. Herek, W. Wohlleben, R. J. Cogdell, D. Zeidler, and M. Motzkus, Quantum control of energy flow in light harvesting, *Nature* 417(6888), 533 (2002)
45. C. Brif, R. Chakrabarti, and H. Rabitz, Control of quantum phenomena: Past, present and future, *New J. Phys.* 12(7), 075008 (2010)
46. N. Dudovich, B. Dayan, S. M. G. Faeder, and Y. Silberberg, Transform-limited pulses are not optimal for resonant multiphoton transitions, *Phys. Rev. Lett.* 86(1), 47 (2001)
47. D. Qi, Y. Zheng, W. Cheng, Y. Yao, L. Deng, D. Feng, T. Jia, Z. Sun, and S. Zhang, Simulating resonance-mediated two-photon absorption enhancement in rare-earth ions by a rectangle phase modulation, *Chin. Phys. B* 27(1), 013202 (2018)